iScience

CellPress
OPEN ACCESS

Article

Long-chain perfluoroalkyl carboxylic acids removal by biochar: Experimental study and uncertainty based data-driven predictive model

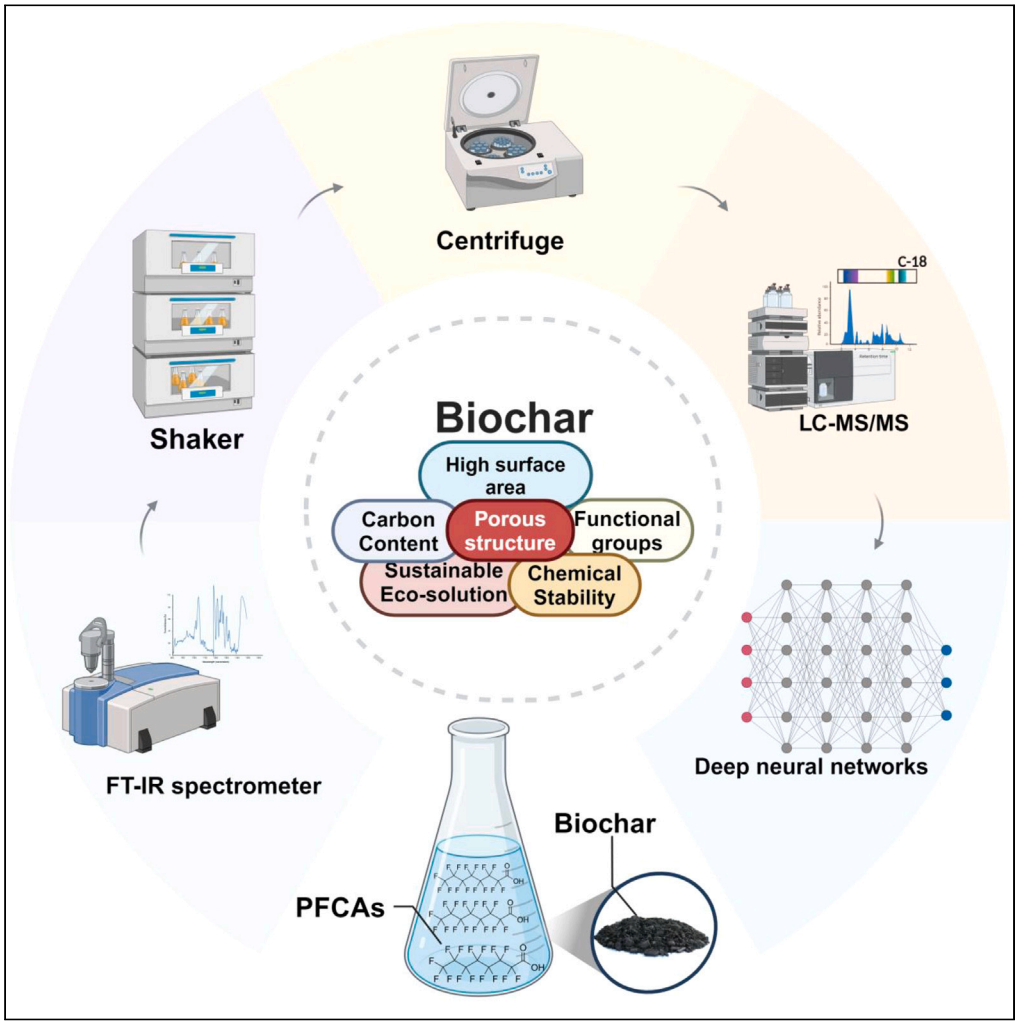

Sepideh Nasrollahpour, Amin Tanhadoust, Rama Pulicharla, Satinder Kaur Brar

satinderbrar@lassonde.yorku.ca

Highlights

Compost biochar achieved up to 90.13% PFDA removal at 500 μg/L concentration

PFDA exhibited higher adsorption rates compared to PFNA due to chain length

Deep neural networks predicted adsorption for single and multi-pollutant scenarios

Key variables for biochar adsorption prediction: time, size, weight, and PFCA concentration

Nasrollahpour et al., iScience *27*, 111140
November 15, 2024
https://doi.org/10.1016/j.isci.2024.111140

iScience

CellPress
OPEN ACCESS

Article

Long-chain perfluoroalkyl carboxylic acids removal by biochar: Experimental study and uncertainty based data-driven predictive model

Sepideh Nasrollahpour,[1] Amin Tanhadoust,[2] Rama Pulicharla,[1] and Satinder Kaur Brar[1,3,*]

SUMMARY

Given the persistence and toxicity of long-chain perfluoroalkyl carboxylic acids (PFCAs) and their rising concentrations, there is an urgent need for effective removal strategies. This study investigated the adsorptive removal of PFCAs, specifically perfluorononanoic acid (PFNA) and perfluorodecanoic acid (PFDA), using biochar derived from wood and compost. Factors such as biochar size, weight, and initial PFCA concentrations were analyzed to assess their impact on adsorption efficiency over time. The adsorption of PFDA and PFNA reached 90.13% and 85.8%, respectively, at an initial concentration of 500 μg/L. Advanced machine learning techniques, specifically deep neural networks, were employed to model adsorption behavior, incorporating noise injection to account for data uncertainties and preventing overfitting. Results demonstrated the superior performance of compost-derived biochar due to its higher aromaticity and functional group availability. The longer chain length of PFDA contributed to its higher adsorption efficiency compared to PFNA.

INTRODUCTION

Perfluoroalkyl carboxylic acids (PFCAs) belong to the extensive family of per- and poly-fluoroalkyl substances (PFAS), which are artificially synthesized organofluorine compounds extensively utilized in polymer additives, fluoropolymer manufacture, fire retardants, food packaging, pesticides, and fabric protection.[1] PFCAs are known for their persistent environmental presence and potential for bioaccumulation, with their toxicity varying significantly across different chain lengths. Studies have shown that shorter-chain PFCAs, such as perfluorobutanoic acid (PFBA), demonstrate acute toxicity with median lethal concentrations (LC50) ranging from 70 to 140 mg L^{-1} for various PFCAs.[2] On the other hand, long-chain PFCAs, including perfluorononanoic acid (PFNA) and perfluorodecanoic acid (PFDA), pose greater risks due to their enhanced persistence and bioaccumulation potential. The Government of Canada has recently classified long-chain perfluoro carboxylic acids (LC-PFCAs), their salts, and precursors as toxic substances, highlighting the need for effective controls and monitoring of these chemicals.[3]

PFCAs are found in numerous water sources worldwide, such as rivers, lakes, seawater, and drinking water. Their levels in these waters can range from a few ng/L to several μg/L at sites with higher contamination.[4] For instance, in the Cape Fear River Watershed in the USA, the average concentration reached 631 ng/L, surpassing the health advisory limits set by the EPA, which is 0.004 ng/L. At an Australian military airbase, levels were notably higher, between 600 and 1,700 μg/L.[4] Among the PFCAs, perfluorooctanoic acid (PFOA) frequently appears in the highest concentrations, with levels reaching up to 11.3 μg/L in Canadian surface waters. Other commonly found PFCAs include perfluorohexanoic acid (PFHxA), perfluorobutanoic acid (PFBA), and PFNA, all of which have been detected at considerable concentrations in various aquatic environments.[4,5]

Traditional treatment methods show limited effectiveness in degrading PFCAs due to the robust C-F bond, their low concentration in water, and their high hydrophilicity. Standard water treatment techniques, including disinfection by free chlorine or ultraviolet (UV) irradiation, are ineffective against these compounds.[6] Their resistance to oxidation by ozone and hydroxyl radicals is higher compared to other micropollutants, attributed to the C-F bond and electron-withdrawing functional groups.[7,8] Biological treatment processes, both aerobic and anaerobic, are capable of breaking C-C bonds; however, they typically result in the formation of shorter-chain compounds rather than complete degradation. Thus, in the absence of advanced technologies, biological wastewater treatment plants (WWTPs) can even lead to an increase in PFCA concentration in treated water compared to untreated water.[9] This demonstrates their resistance to biological treatment and formation through the biodegradation of precursor compounds.[10] Adsorption has been identified as an effective and preferred method for the extraction of PFCAs from wastewater due to its ability to capture contaminants at very low concentrations, which is crucial given the trace amounts of PFCAs typically found in water systems.[11] Unlike conventional degradation methods that struggle with the robust C-F bond,

[1]Department of Civil Engineering, Lassonde School of Engineering, York University, Toronto, ON M3J 1P3, Canada
[2]Department of Civil Engineering, Isfahan University of Technology (IUT), Isfahan, Iran
[3]Lead contact
*Correspondence: satinderbrar@lassonde.yorku.ca
https://doi.org/10.1016/j.isci.2024.111140

adsorption relies on the interaction between the adsorbent material and PFCA molecules, facilitating their removal from water without requiring complex reactions or high energy inputs.[12] Several adsorbents, including resin,[13] activated carbon (AC),[14,15] chitosan,[16] and hydrotalcite,[17] have been explored for this purpose. For instance, the research conducted by Zhang et al. demonstrated that the chitosan biosorbent exhibited a sorption capacity as high as 5.5 mmol/g for perfluorooctane sulfonate (PFOS) at an equilibrium concentration of 0.33 mmol/L, significantly surpassing many traditional adsorbents.[15] Although some research has shown effective removal of PFCAs using these methods, they are often considered either too costly or inefficient.[18] The Environmental Protection Agency (EPA) discussed the costs of treatment technologies, such as GAC, for removing PFAS from water during the 2020 Annual Conference. The total yearly expense for treating PFAS with GAC is estimated to be around $48 million, serving over 2,000 households. From the perspective of inefficiency, Pattarawan[16] investigated the use of granular activated carbon (GAC, Filtrasorb 400) and various resins (XAD4, PFA300, and Dow Marathon A) for removing PFHxA, PFHpA, and PFOA from the effluents of industrial wastewater treatments related to polytetrafluoroethylene production. Despite ng/L concentration of PFCAs, commercial granular AC was identified as the least effective adsorbent, achieving maximum adsorption capacities of about 150 ng/g for PFOS and 200 ng/g for PFOA. Similarly, Schaefer et al.[19] found that PFCs could easily bypass GAC beds in German wastewater treatment plants, indicating that commercial ACs may be unsuitable for PFCA removal in wastewater. Consequently, there is an ongoing need to identify more effective adsorbents for this purpose.

Given the challenges mentioned, there is a continuous search for more efficient methods and improved absorbents for PFCAs removal. Biochar, a carbon-rich substance produced through pyrolysis, is frequently compared to granular activated carbon (GAC) due to their similar attributes, although their production methods are markedly different.[20] The production of GAC typically involves high pyrolysis temperatures (900°C–2000°C) and additional physical or chemical activation, rendering their production both expensive and energy-intensive.[21] In contrast, biochar is produced through a less energy-demanding process, utilizing lower pyrolysis temperatures (<1000°C) compared to commercial activated carbons, and often does not require an activation step. Consequently, these factors make biochar a preferable adsorbent.[22] A study by Liu et al. (2021) investigated the use of reed straw-derived biochar (RESCA) for the efficient removal of short-chain PFASs. The study demonstrated that RESCA, particularly when pyrolyzed at 900°C for 5 h, achieved exceptional removal efficiencies exceeding 92% for short-chain PFASs such as perfluorobutanoic acid (PFBA) and perfluorobutanesulfonic acid (PFBS) at environmentally relevant concentrations (e.g., 1 μg/L). The high adsorption performance of RESCA was attributed to its hydrophobic surface and uniform distribution of mesopores (2–10 nm), which facilitated rapid adsorption kinetics and enhanced adsorption capacities compared to conventional granular activated carbon (GAC).[23] These findings underscore the potential of biochar as a viable and scalable solution for PFCA removal, providing a critical context for the current study's focus on biochar's application in water treatment technologies.

In this study, the potential of biochar as an adsorbent for long-chain PFCAs, specifically PFNA and PFDA, was explored, addressing the gap in its application for PFCAs. Uncertainty analysis was incorporated into the experimental design, and machine learning models were used to predict adsorption efficiency, accounting for data uncertainties. The study examined the influence of the size and weight of biochar, PFCA concentrations, and time intervals on adsorption efficiency. Predictive models were developed for both single and multiple pollutants, aiming to provide robust predictions and guide the optimization of biochar-based treatment systems for effective PFCA removal.

EXPERIMENTAL PROGRAM

Chemicals and materials

Two types of biochar, both sourced from CHAR Technologies Inc. Toronto, Canada were utilized. One type was derived from composted food waste and the other from pine wood shavings.

Perfluorononanoic acid ($C_9HF_{17}O_2$, 464.078 g/mol) and perfluorodecanoic acid ($C_{10}HF_{19}O_2$, 514.09 g/mol) were both obtained with a purity of 97% from Thermo Fisher Scientific. Stock solutions of these compounds were prepared in methanol, sourced from Fisher Scientific.

All experiments were conducted using deionized water with a resistivity of 18.0 MΩ cm, produced by a Milli-Q System (Milford, MA, USA).

Biochar characterization

To evaluate the impact of biochars particle size on adsorption efficiency, the biochars were ground and sifted into four different size ranges: 0.063–0.074 mm, 0.125–0.149 mm, 0.250–0.297 mm, and 0.841–1 mm. These were then stored in sealed containers until used.

Fourier transform infrared spectroscopy (FTIR) was utilized to investigate the surface chemical composition of the produced biochar particles, specifically focusing on the functional groups involving carbon (C), nitrogen (N), oxygen (O), and hydrogen (H). The biochar samples were subjected to FTIR (Bruker Alpha-P FTIR Spectrometer, USA) under ambient conditions (24 ± 2°C). The spectral range of 4000 to 400 cm−1, with a resolution of 4 cm−1, enabled the precise identification of the different chemical entities present on the surface of the biochar.

The quantification of total C, N, H, and sulfur (S) in the biochar samples was performed using a Thermo Flash Smart V Elemental Analyzer. This instrument operates on the principle of dynamic flash combustion, where the biochar samples are combusted in a high-temperature furnace. During this process, the samples are oxidized, and the resulting gases are then separated and quantified using a gas chromatography system coupled with a thermal conductivity detector (TCD).

Screening and selection of biochar

To determine the efficacy of selected biochars in adsorbing PFCAs, a screened experiment was designed. Initially, 25 mg of each biochar, with a size range of 125–149 μm, was added to flasks containing 25 mL of MilliQ water. These mixtures were then spiked with target PFCAs with

varying concentrations, including 10, 100, and 500 μg/L, to simulate low to high contamination scenarios. The mixtures were incubated at 150 rpm for 24 h. Subsequently, the mixtures were centrifuged at 4000 rpm for 10 min to separate the biochar from the aqueous phase. The adsorbed concentration of PFCAs treated with biochar in water was determined using liquid chromatography-mass spectrometry (LC/MS).

Assessing the adsorptive kinetics of perfluoroalkyl carboxylic acids

Following the screening of the biochar having higher adsorption efficiency, the kinetics of selected adsorption capacity were analyzed to observe the trend of adsorption over time and to optimize the adsorption period. For each trial, 25 mg of the select biochar was introduced into a flask containing 50 mL of MilliQ water. The solution was then spiked with PFCAs to establish a contaminant concentration of 100 μg/L. The flasks were agitated at a speed of 150 rpm continuously for 72 h to facilitate the adsorption process. Samples were taken at intervals of 0, 0.5, 1, 3, 6, 21, 24, 48, and 72 h to determine the changes in adsorption capacity over time. After each interval, the samples were centrifuged at 1788 x g for 10 min to separate the biochar from the solution. The supernatants were then collected for analysis by LC/MS.

Batch sorption tests

The design of the adsorption experiments to evaluate the effectiveness of biochar was conducted using response surface methodology (RSM) and the central composite design (CCD) approach, which are particularly advantageous over the traditional one variable at a time (OVAT) method. RSM and CCD allow for the efficient exploration of interactions between multiple variables, which can significantly save time and resources by reducing the number of experimental runs required. CCD allows for the estimation of not just first-order (linear) effects but also second-order (quadratic) effects and interactions between variables. This capability is essential for developing a thorough understanding of the response surface, thus enabling the optimization of outcomes in complex systems. This contrasts sharply with OVAT, which can be time-consuming and less effective in understanding variable interactions because it investigates one variable at a time without considering inter-dependencies, often resulting in more experimental runs to reach similar conclusions.[24,25]

In this study, various parameters were focused on, including biochar particle size ranging from 0.063 to 1 mm across four categories (0.063–0.074, 0.125–0.149, 0.250–0.297, and 0.841–1 mm), concentrations of PFCAs varying between 10 and 200 ppb, both in single and mixed contaminant scenarios (PFNA and PFDA), and biochar quantities ranging from 25 to 100 mg. The final experiment design is shown In Table S1. In each experiment, PFCAs were spiked into 50 mL of Milli-Q water in flasks. The flasks were then incubated in a shaking incubator at 150 rpm, at 25°C. The biochar-treated samples were collected at intervals of 0.5, 1, 2, 3, 5, 8, and 10 h. Then, biochar and solutions were separated through centrifugation at 4000 rpm for 10 min. The samples were then analyzed using LC-MS to determine the concentrations of PFCAs.

Sample extraction and analysis (perfluoroalkyl carboxylic acid analysis by liquid chromatography-mass spectrometry/mass spectrometry)

The quantification of PFCA concentrations was carried out utilizing an ACQUITY M-class UPLC system (Waters) coupled with a ZenoToF 7600 (Sciex) mass spectrometer. For analysis, 5 μL of each sample was injected into the LC-MS/MS system, which was equipped with a C18 column (Kinetex 2.6 μm XB-C18 100 Å, LC Column 50 × 0.3 mm, Phenomenex). The system operated at a flow rate of 20 μL/min. The initial mobile phase composition was 99% solvent A (water with 0.1% formic acid) and 1% solvent B (acetonitrile with 0.1% formic acid). This was adjusted over 5 min to reach 100% solvent B, and then returned to 1% within the next minute. The mass spectrometer's ion optics functioned in the negative ion electrospray mode, set with a spray voltage of −4500 V. The settings for ion source gases 1 and 2 were maintained at 20 psi. Gas 1 and gas 2 are parameters in the mass spectrometer software that controls the flow of nitrogen used for the desolvation of chemicals. Desolvation is a critical process where compounds transition from the liquid phase to the gas phase within the ion source. Additionally, curtain gas pressure was set at 35 psi, collision gas at 7 psi, a source temperature of 150°C, and a column temperature set at 50°C. Quantitative measurements were conducted using high-resolution multiple reaction monitoring (MRM-HR), and the corresponding transitions were recorded, including precursor ion m/z values and product ion start/stop m/z values, as detailed in Table S2.

Machine learning

Artificial neural networks (ANNs) mimic the human brain's neuron network to process information. These models, known for their parallel and dynamic structure, handle both experimental and theoretical data without needing initial transformation or assumptions. The core algorithm, the multilayer perceptron, directs information through input, hidden, and output layers. Deep neural networks (DNNs), with their multiple layers, excel in analyzing complex patterns in large datasets, making them ideal for predictive environmental modeling. DNNs enhance the understanding and prediction of environmental processes. In this study, advanced computational techniques such as machine learning (ML) are crucial due to the complexity and variability of PFCA adsorption onto biochar. ML's capability to manage non-linear and complex data makes it a valuable tool in environmental engineering, especially for modeling biochar's adsorptive properties.[26,27]

Evaluation metrics of artificial neural networks

The efficacy of ANNs is assessed through statistical metrics that evaluate the model's precision and accuracy. These metrics include the co-efficient of determination (R^2), Root-Mean-Square Error (RMSE), and Mean Absolute Error (MAE). R^2 measures the model's fit, with values

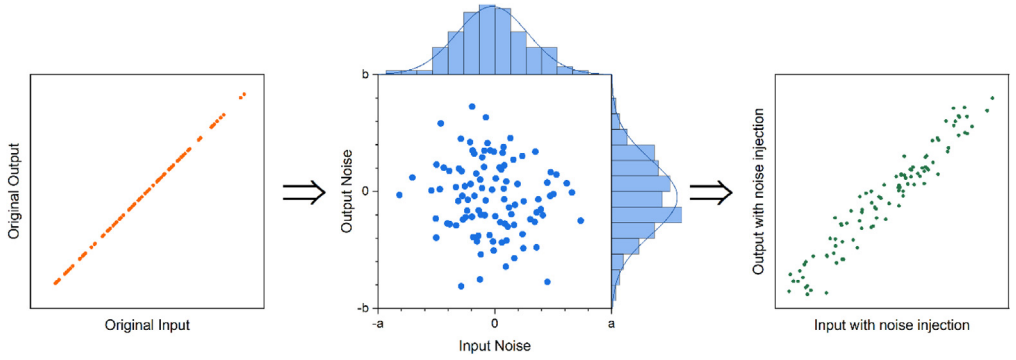

Figure 1. Concept of noise injection to data

ranging from 0 to 1, allowing for comparison across different datasets. RMSE and MAEgauge the deviation between predicted and actual values. Sensitivity analysis examines the impact of varying input variables, such as data noise levels, the number of neurons in each layer, and the type of activation function used, on model output.[28] High R^2 and low RMSE values indicate robust predictive capability and accuracy. The mathematical expressions for these metrics are detailed in Table S3, facilitating the optimization of ANNs for improved predictive accuracy in scientific and engineering applications.[29]

Noise injection and overfitting management

Managing noise injection and overfitting within the framework of DNNs is pivotal, especially when modeling the intricate process of adsorption in this study. Given the inherent uncertainties in experimental data and the complexities of environmental and physical-chemical interactions, a refined approach to model training, which accounts for real-world variabilities, is essential.[30,31]

To reduce overfitting, the study employs a combination of dropout layers and regularization techniques. Dropout layers randomly disable a proportion of neurons during training, preventing the model from depending too heavily on any individual neuron and thus promoting more distributed and generalized learning.[32] The dropout rate is chosen to balance the need for model complexity with the risk of overfitting. Regularization techniques, such as L1 and L2 regularization, add a penalty on the magnitude of network weights, discouraging overly complex models that could memorize the training data, including its noise and outliers.[33]

On the other hand, incorporating noise into the training process simulates the unpredictable nature of real-world data, enhancing the model's robustness and its ability to generalize from the training set to unseen data. This study adopts a strategic approach to noise injection, guided by empirical data uncertainties. Parameters such as μ (mean) and σ (standard deviation) are meticulously selected based on the experimental errors observed in the PFCA adsorption data. For instance, if experimental measurements of adsorption efficiency exhibit a standard deviation of σ, noise is generated with a matching σ to mimic the observed data variability. This alignment ensures that the noise-injected data faithfully represent the experimental conditions, including any errors or variations.

The selection of μ and σ is not arbitrary but grounded in the statistical analysis of experimental errors. By analyzing the dispersion and central tendency of errors in the experimental data, these parameters are tuned to reflect the natural fluctuations in the data accurately. This methodical selection process ensures that the DNN models are exposed to and learn from data that closely mimic the real experimental conditions, including the inherent uncertainties.

The concept of noise injection into data is illustrated in Figure 1. Through strategic noise injection, grounded in the statistical properties of experimental errors, and diligent overfitting management, this study not only enhances the predictive capability of DNNs in environmental modeling but also ensures that the predictions made are robust, reliable, and reflective of real-world complexities. This advanced modeling approach significantly contributes to our understanding and prediction of PFCA adsorption processes, offering a nuanced tool for environmental research and management.

Proposed predictive model and performance

This study utilized diverse DNN architectures to identify the optimal network structure, as shown in Figure 2. The activation function employed was real, and a learning rate of 0.001 was chosen to enhance model performance. A consistent batch size of 64 was maintained across all training and validation phases, ensuring uniformity. The training set, derived from X experimental observations, involved five principal independent parameters, namely Time, $PFNA_0$, $PFDA_0$, Biochar Size, and Biochar Weight, predicting $PFNA_t$ and $PFDA_t$ outcomes as demonstrated in Figure 2. These inputs and outputs, along with their minimum and maximum values, are detailed in Table 1, with a data split of 70% for training and 30% for validation. To combat overfitting, a dropout rate of 10% was implemented, and noise injection techniques were applied post-normalization, further enhancing model robustness.

A linear regression comparing the predicted and actual values indicated the model's accuracy in estimating the adsorption efficiency, significantly contributing to our understanding and optimization of biochar-based water treatment solutions, as shown in Figure 3. Also, the values of evaluation metrics for the proposed predictive model is shown in Table 2 for datasets with and without noise as well as train

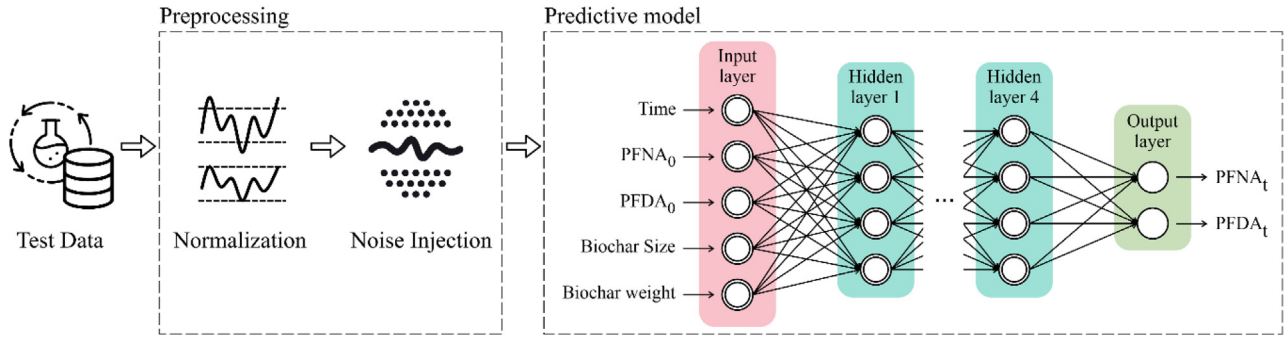

Figure 2. Workflow of proposed predictive model

and test phases. The approach outlined underscores the transformative potential of DNNs in environmental remediation efforts, particularly in water purification processes plagued by PFCA contamination. By leveraging machine learning, particularly DNNs, this study presents a paradigm shift from traditional experimental methodologies to a more efficient, data-driven predictive modeling framework. This shift not only enhances our understanding of PFCA adsorption dynamics but also paves the way for the development of more effective, sustainable water treatment technologies.

RESULTS AND DISCUSSION

Characteristics of biochars

The elemental analysis of biochars and the conditions of their pyrolysis are presented in Table 3. The compost-based biochar, pyrolyzed at 800°C, likely contained a higher proportion of aromatic carbon structures compared to the wood-based biochar produced at 600°C. A correlation was observed between aromaticity and the biochar's ability to adsorb pollutants through π-π interactions, which was crucial for the capture of PFAS compounds due to their carbon-fluorine bonds.[34] The degree of carbonization was indicated by the H/C ratio; enhanced aromaticity and reduced volatile matter are suggested by the lower ratios in both biochars, contributing to the adsorption of PFAS. The C/N ratio indicateds the availability of carbon sites for adsorption; a higher ratio in compost-based biochar implied more carbon surface area available for PFAS interaction, thus enhancing its uptake from water.[34,35] In light of these considerations, the compost-based biochar was more effective for the adsorption and removal of PFCAs compared to its wood-based counterpart.

The FTIR results of selected biochars, as shown in Figure 4, indicate a diverse array of functional groups with distinct absorption peaks. The observed broad band between 4000 and 3000 cm^{-1} was characteristic of hydroxyl group O-H stretching vibrations, indicative of hydrogen bonding potential, and present in both biochar samples. Peaks at 445 cm^{-1} and 870 cm^{-1} suggested the presence of aromatic structures, attributed to out-of-plane bending and deformation of aromatic C-H bonds, respectively. These features were significant, as they point to the type and degree of aromatic condensation within the biochars.[36]

Notably, the compost-derived biochar exhibited a pronounced peak at 1590 cm^{-1}, corresponding to C=C stretching vibrations within aromatic rings, which denoted a higher level of aromaticity in comparison to the wood-derived biochar. This enhanced aromaticity suggested a potential for more effective π-π interactions, which was crucial for the adsorption of planar aromatic contaminants. The peak appearing at 1410 cm^{-1} was likely representative of carboxylic functional groups, either from the symmetric stretching of carboxylate salts or asymmetric stretching of carboxylic acid dimers. This indicated a substantial presence of carboxyl groups in the compost-derived biochar, contributing to its adsorptive capabilities.[37]

Table 1. Ranges of input and output variables

Variable	Unit	Minimum	Maximum
Input			
Time	hour(s)	0.5	10
$PFNA_0$	Ppb	0	133.65
Output			
$PFDA_0$	Ppb	0	124.6
Biochar size	Categorized	1	4
Biochar weight	mg	25	100
$PFNA_t$	ppb	0	103.17
$PFDA_t$	ppb	0	106.685

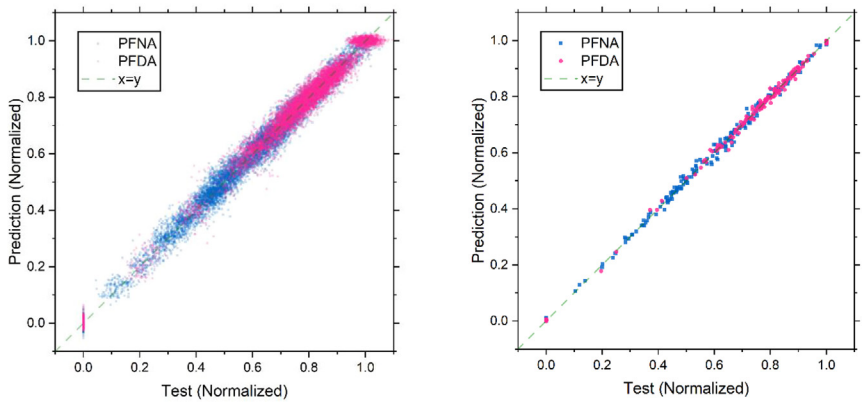

Figure 3. Predicted versus actual normalized values of adsorption in the train and test phases

A peak around 1000 cm^{-1}, consistent with C-O stretching vibrations, alluded to ethers or alcohol functional groups, further affecting the biochar's adsorption characteristics by enhancing its polarity. The FTIR analysis suggested that compost-derived biochar could be a better adsorbent due to its higher aromaticity and the increased availability of functional groups, compared to wood-derived biochar.[36]

Screening and selection of biochar

Table 4 depicts the efficacy of different biochars for the remediation of PFCAs in three varying initial concentrations (10, 100, and 500 μg/L). At the lowest concentration (10 μg/L), compost-based biochar demonstrated a removal efficiency of 43.08% for PFNA, surpassing wood-based biochar, which achieved only 14.73%. This trend continued for PFDA removal, with compost biochar recording a removal efficiency of 62.13%, compared to 23.91% by wood biochar. At 100 μg/L, compost biochar removed 52.03% of PFNA and 71.34% of PFDA, whereas wood biochar exhibited removal rates of 36.23% and 42.53%, respectively. At the highest concentration of 500 μg/L, compost biochar removed 85.8% of PFNA and 90.13% of PFDA, markedly outperforming wood-based biochar, which showed removal efficiencies of 46.76% for PFNA and 51.81% for PFDA.

The superior performance of compost biochar in PFCA adsorption can be attributed to its origin and distinct source material compared to wood biochar. This difference in source material contributed to variations in structural and chemical properties. Moreover, a higher pyrolysis temperature in compost biochar can lead to a larger carbon surface area and a higher carbon-to-nitrogen ratio. Additionally, the presence of more functional groups in compost biochar, as previously mentioned, enhanced its adsorption capabilities.[38]

Functional groups such as hydroxyl, carboxyl, and carbonyl groups on the surface of biochar provide active sites for the adsorption of contaminants. These groups can form hydrogen bonds, electrostatic interactions, and π-π interactions with PFCA molecules, thereby increasing the adsorption capacity. The aromaticity of compost-based biochar, indicated by FTIR analysis showing higher peaks associated with aromatic and carbonyl groups, suggests the presence of π-conjugated systems. These systems facilitate π-π electron donor-acceptor interactions, which are particularly effective in adsorbing aromatic compounds such as PFCAs.[36]

The removal efficiency for both biochars increased with the concentration of PFCAs due to the increasing availability of PFCA molecules at higher concentrations, which facilitated greater interaction with the biochar's active sites. The enhanced aromaticity potentially facilitated π-π electron donor-acceptor interactions with PFCA molecules, a mechanism supported by FTIR analysis revealing higher peaks associated with aromatic and carbonyl groups—functional groups known for their affinity toward PFCA compounds. Based on these results, compost-based biochar was chosen to continue this study.

Effect of equilibration time and different chain lengths of perfluoroalkyl carboxylic acids on sorption

Figure 5 illustrated the adsorptive kinetics of PFNA and PFDA on compost-derived biochar to understand the equilibrium time of removal. Initially, both PFCAs exhibited a rapid uptake, due to the availability of abundant active sites on the biochar surface. This initial phase typically reflected the external surface adsorption or instantaneous adsorption stage. PFDA demonstrated a higher adsorption efficiency compared to

Table 2. Evaluation metrics for proposed predictive model

Dataset	Original			Noise-injected			Train	Test
Output	PFNA	PFDA	All	PFNA	PFDA	All	All	All
R2	0.9985	0.9997	0.9993	0.9898	0.9948	0.9931	0.9968	0.9962
RMSE	0.0125	0.0090	0.0109	0.0293	0.0265	0.0279	0.0261	0.0319
MAE	0.0088	0.0057	0.0073	0.0222	0.0196	0.0209	0.0177	0.0243

Table 3. Physicochemical properties of different types of biochar

	Biochar Pyrolysis		Elemental analysis (%)				Elemental ratios	
Type of biochar	Residence time (min)	Temperature (°C)	C	H	N	S	H/C	C/N
Wood -Based	40	600	46.6	6.39	2.92	0.6	0.14	15.99
Compost-Based	30	800	49.8	7.96	1.88	0.3	0.16	26.56

PFNA over 72 h. Initial adsorption rates displayed a significant disparity; within the first hour, PFDA achieved 25.34% compared to PFNA, which reached 6.64%. This rapid initial adsorption of PFDA can be attributed to its longer carbon chain and molecular structure, which enhance its hydrophobic interactions with biochar. The longer carbon chain length exhibited better compatibility with the biochar's surface properties, leading to stronger and more numerous adsorption interactions.[39] As the interaction progressed over 72 h, the adsorption rates for both PFCAs converged, albeit maintaining a significant gap—PFNA reached 55.73%, while PFDA achieved 76.45%. The decreasing rate disparity over time suggested an eventual saturation of biochar's adsorptive sites, a common phenomenon in sorbent-sorbate interactions.[40]

Similar studies, such as Guo W et al.,[41] have also reported on the kinetics of PFAS adsorption onto different types of biochars. These studies generally showed that adsorption efficiency was influenced by the characteristics of both the biochar (such as surface area, porosity, and functional groups) and the PFCAs (chain length and head group). Leung S et al.[35] demonstrated that longer-chained PFCAs exhibited higher adsorption capacities, corroborating the results observed in this study. Previous studies have shown that the Kd value (distribution coefficient), which indicated the affinity of a substance for a sorbent, increased with the length of the perfluorinated chain. This was believed to be due to stronger hydrophobic interactions that were characteristic of longer PFAS chains. The perfluorinated tail, which has a substantial surface area, contributed to weak van der Waals forces, and the energy needed to form a cavity in water for a PFCA molecule went up with each added CF2 group. This was consistent with findings by Du et al., who suggested that the energy to create these water cavities and van der Waals forces played a significant role for longer-chained PFAS, those with more than six carbons, compared to shorter ones. Our results aligned with this chain length dependency, reinforcing the idea that hydrophobic interactions were a key force behind the sorption of PFCAs to biochars.[12]

Based on Figure 5, a sharp increase in adsorption efficiency was observed during the initial 8 to 10 h, which led to the selection of a 0 to 10-h time frame for the experiments. This result aligned with the findings of Zhang et al.,[42] who reported that the kinetics equilibrium for PFOS and PFOA adsorption by biochar occurred within 6–10 h.

Test results versus predictions

In the experiments, 30 test runs were conducted, considering variables including biochar size, biochar weight, and PFCA concentration. The results of all these 30 tests, along with model predictions, are illustrated in Figure S1. Each figure was labeled according to the test number, which can be found in the corresponding table along with other variables. The data revealed that the adsorption capacities of compost-derived biochar for PFNA and PFDA were markedly high, demonstrating an impressive removal efficiency that exceeded 60% across all tests conducted under various conditions.

The alignment between experimental outcomes and the AI model's predictions was strikingly precise. This close correspondence, depicted in Figure S1 associated with these tests, not only validated the AI model's utility in simulating biochar's adsorption behavior but also underscored the potential of predictive analytics in optimizing biochar application for environmental remediation.

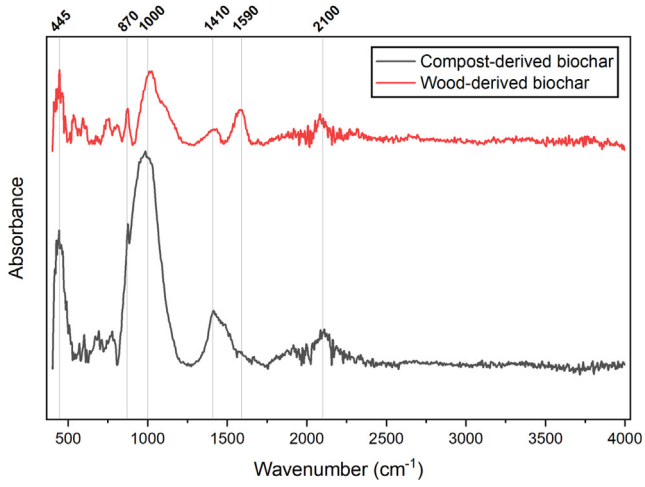

Figure 4. FTIR spectra comparison between compost- and wood-derived biochars

Table 4. Comparative removal efficiencies of two types of biochars for PFCAs at various initial concentrations

Initial concentration (μg/L)	10		100		500	
Type of PFCA	PFNA	PFDA	PFNA	PFDA	PFNA	PFDA
Wood Biochar Removal (%)	14.73	23.91	36.23	42.53	46.76	51.81
Compost Biochar Removal (%)	43.08	62.13	52.03	71.34	85.8	90.13

Based on the Figure S1, the majority of PFNA and PFDA removal by biochar occurs within the initial 2 h, demonstrating a rapid uptake phase. After this period, the adsorption curve flattened. This pattern indicated that the majority of active adsorption sites on biochar were quickly utilized, with limited additional adsorption capacity available after this initial period, highlighting the importance of the initial contact time in optimizing biochar's effectiveness for PFCA removal.

There was an inverse correlation between the particle size of biochar and its adsorption efficacy. An analysis comparing experiments 9 and 10, utilizing identical masses of biochar, revealed that a reduction in particle size from 841 to 1000 μm to 125–149 μm resulted in a significant increase in adsorption efficiencies for PFNA and PFDA, improving from 22% to 60%–42% and 71%, respectively. This observation underscored the critical importance of the surface area, as smaller biochar particles provided a more extensive interface for PFCA interaction, thereby increasing the adsorption rate.

Conversely, further reduction in biochar particle size from 125-149 μm to 63–74 μm, as investigated in experiments 11 and 12, did not elicit a corresponding increase in adsorption efficiency. This suggested the existence of an optimal particle size threshold, beyond which further reduction did not yield significant improvements in adsorption performance. This finding indicated that while the increase in surface area associated with smaller particle sizes can enhance adsorption up to a point, there existed a limit to the benefits of size reduction, highlighting the need for a strategic approach to biochar size optimization in adsorption processes.

Based on experiments 4, 8, 11, 16, and 20 where the concentrations of PFNA and PFDA were similar, it was observed that PFDA exhibited higher adsorption rates than PFNA, which can be attributed to differences in chain length, consistent with prior studies. The distribution coefficient (Kd) increased with the length of the perfluorinated chain, a phenomenon that can be tied to enhanced hydrophobic interactions seen with longer PFAS chains.[43] The extended perfluorinated chains, characterized by their large surface area and minimal van der Waals forces, led to an increase in the free energy required for cavity formation to dissolve PFCAs in water, with each addition of a CF2 (difluoromethylene) unit.[44] This pattern of chain length influencing adsorption supported the theory that hydrophobic interactions played a pivotal role in the adsorption of PFCAs onto biochars, as noted in prior research. Fabregat-Palau et al.[45] observed a direct correlation between the addition of fluorinated carbons to the alkyl chain and an increase in PFAS hydrophobicity (as indicated by log K_{OW}). Their findings further affirmed that adsorption rates for PFAS increased with longer fluorinated chains, suggesting that longer-chained PFAS have a stronger affinity for carbon-rich materials due to hydrophobic interactions, with electrostatic forces playing a lesser role in the adsorption.

Sensitivity analysis

Single-pollutant

The sensitivity analysis of PFNA and PFDA adsorption efficiency, considering initial PFCA concentration, biochar weight, and biochar particle size, is depicted in Figures 6 and 7 for 0.5, 2, and 10 h. These figures were segmented based on varying biochar sizes, where white dotted lines represent the percentage removal efficiency (%), and black lines illustrate the adsorption quantity (ppb).

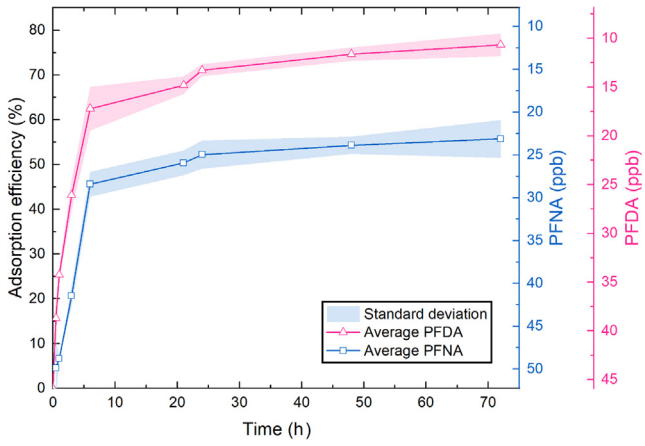

Figure 5. Adsorption kinetic curves of PFNA and PFDA by compost-derived biochar

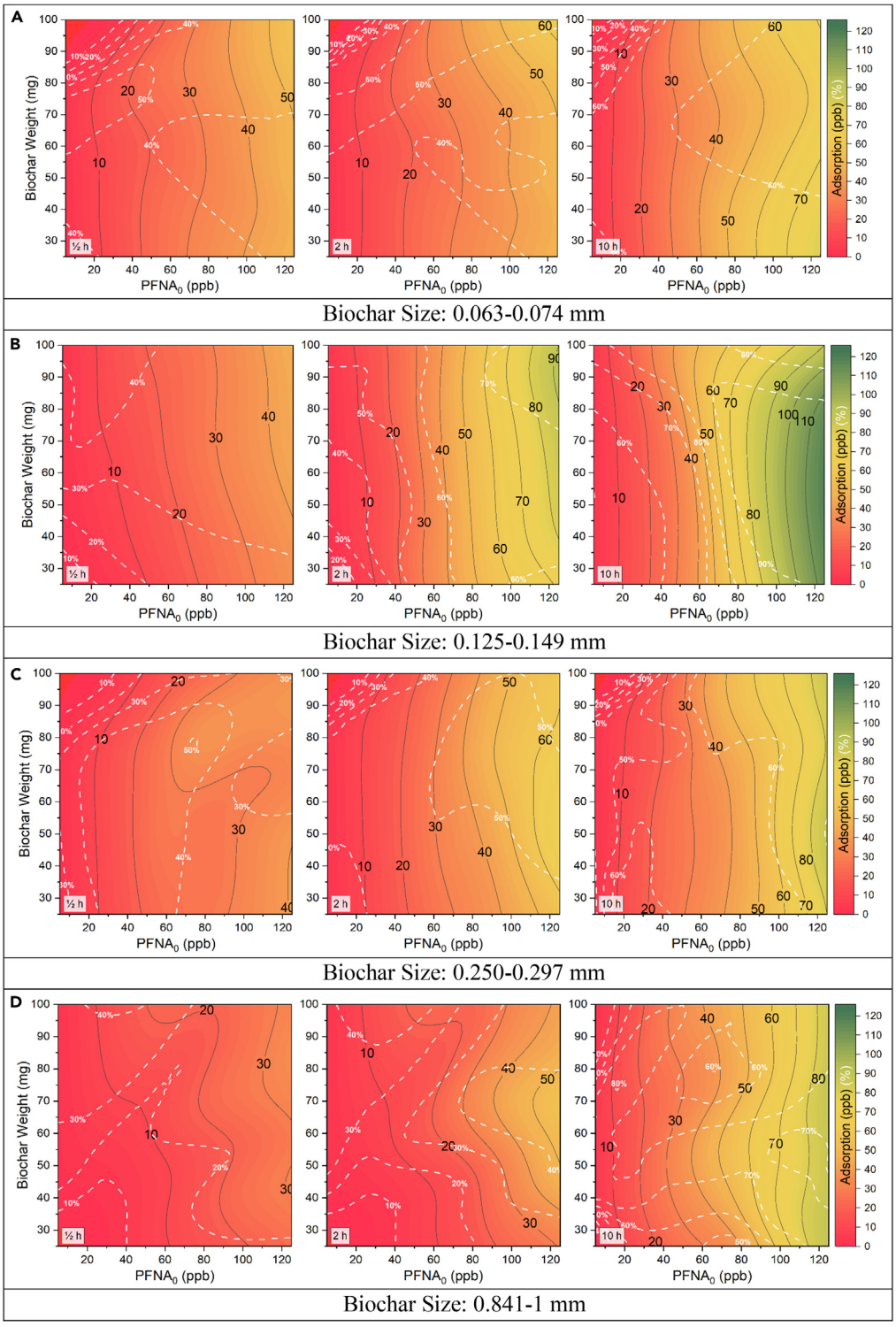

Figure 6. Analysis of PFNA adsorption efficiency sensitivity with respect to different variables

A comparison in Figures 6 and 7 under identical conditions showed that PFDA has a higher adsorption capacity than PFNA. For example, within a biochar size range of 0.125–0.149 mm, the initial 30-min interval demonstrated up to 40% adsorption for PFNA, whereas PFDA achieved a removal efficiency of up to 70%. This differential adsorption capacity can be attributed to the molecular

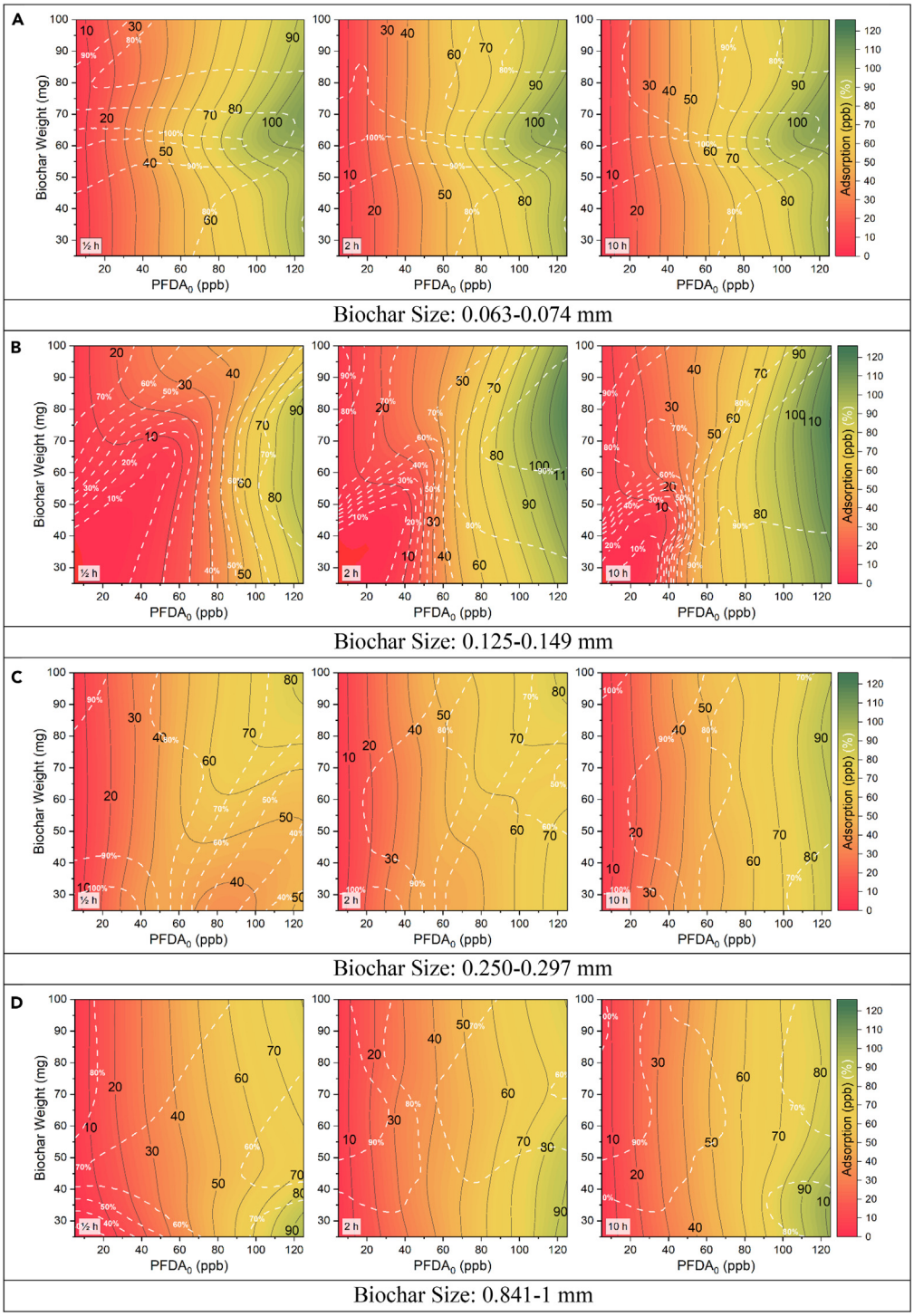

Figure 7. Analysis of PFDA adsorption efficiency sensitivity with respect to different variables

structure differences between PFNA and PFDA, which were mentioned previously. The longer carbon chain of PFDA could potentially enhance hydrophobic interactions and π-π electron donor-acceptor interactions with the biochar, leading to higher adsorption rates initially. These variations in adsorption performance between the two PFCAs diminished over time. For instance, with a biochar size range of 0.841–1 mm, the adsorption of PFNA and PFDA converged to 80% and 100%, respectively, after 10 h. Over time, as the

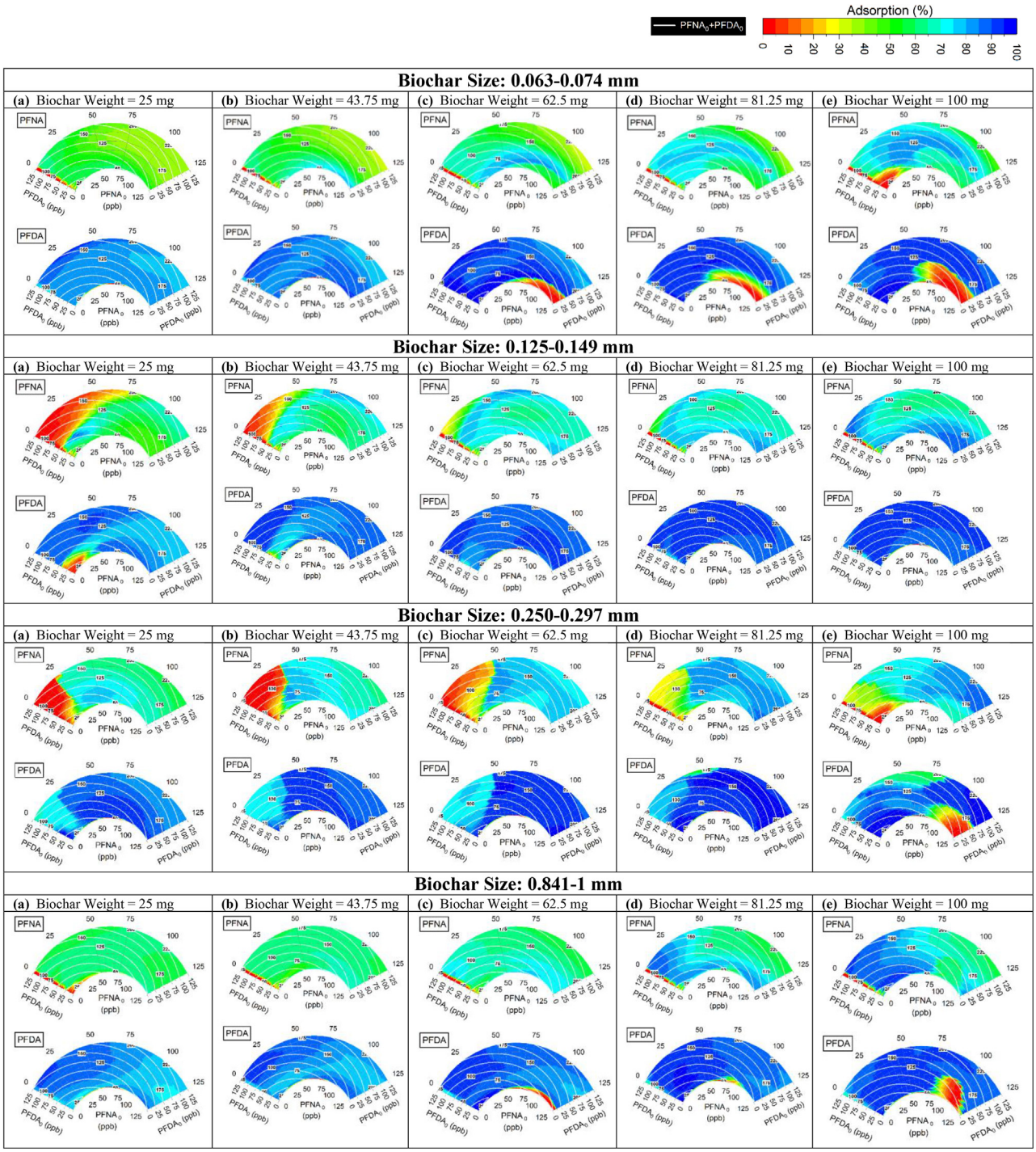

Figure 8. Sensitivity analysis of adsorption efficiency for different sizes of biochar in conditions with multiple pollutants

available adsorption sites on the biochar become occupied, the rate of adsorption slows, and the disparity in removal efficiency between PFNA and PFDA decreases. This observation was consistent with the adsorption isotherms that typically plateau as a system approaches equilibrium.

The reduction of biochar particle size from the range of 0.841–1 mm to 0.125–0.149 mm correlated with an increase in adsorption, attributed to the higher surface area. However, this trend did not continue with the further decrease in size to 0.063–0.074 mm, where an increase in adsorption is not observed. Theoretically, according to the DLVO theory, as the biochar particles become smaller, the surface area-to-volume

ratio grows, which should provide more sites for adsorption. Nevertheless, DLVO theory—which clarifies the interparticle forces within colloids, including attractive van der Waals forces and repulsive electrostatic forces—indicated a more complex outcome for extremely small particles. The growth in van der Waals forces may accidentally cause smaller particles to clump together, reducing the effective surface area accessible for adsorption. At the same time, the increased surface charge on small particles can amplify electrostatic repulsion, blocking the adsorbate-adsorbent interactions necessary for the efficient adsorption of PFCAs. Thus, the size of 0.125–0.149 mm for biochar is an optimal particle size that maximizes adsorption efficiency by balancing the increased surface area with the effects of interparticle forces.[46]

Multi-pollutant

The sensitivity analysis of adsorption efficiency under conditions with multiple pollutants is illustrated in Figure 8, categorized according to biochar size. The graphs are displayed using polar contour plots, a method for presenting multivariate data on a two-dimensional graph. The axes on charts radiate out from the center and each radar chart is divided into two semicircles. PFNA adsorption is represented by the upper half of each radar chart, and PFDA adsorption is represented by the lower half by percentage. The angle (θ) corresponded to the initial concentration of PFNA (ppb), and the radius of the charts shows the initial concentration of PFDA (ppb). In each figure, panels (a) through (e) represent biochar weights from 25 to 100 mg. Within each panel, the white contour lines demonstrate the combined initial levels of PFNA and PFDA. Adsorption percentages are indicated by a color gradient, with red tones showing lower adsorption efficiency and blue tones representing higher efficiency.

PFDA exhibits a relatively stable color spectrum and shows less variation in response to changes in biochar quantity and particle size compared to PFNA, which transitions from red to blue, indicating a higher level of effectiveness. This implies that removing compounds with shorter chain lengths, such as PFNA, is a more challenging process, thereby underscoring the importance of condition optimization for such compounds. By comparing the various sizes and their adsorption levels, it was clear that biochar particles ranging from 0.25 to 0.297 mm were the most effective, capturing the most contaminants across various setups and concentrations. The ideal quantity of biochar for maximizing PFDA adsorption was 43.75 mg, which performed better in the competitive adsorption process involving PFNA. Additionally, the optimum amount of biochar for PFNA was 81.2 mg.

Since PFCAs are considered "forever chemicals," this study presented an effective approach for their removal from aquatic environments. The next step in this research will focus on methods for degrading these contaminants alongside their adsorption and removal.

Conclusion

The compost-derived biochar was effective in adsorbing long-chain PFCAs achieving a removal efficiency of up to 90.13% for PFDA at a concentration of 500 μg/L in 24 h. In contrast, wood-derived biochar achieved a maximum removal efficiency of 51.81% for PFDA under the same conditions. Most of the adsorption occurred within the first 3 h, during which PFNA and PFDA reached 20.65% and 43.15%, respectively. At each time point, PFDA exhibited higher adsorption efficiency than PFNA due to its longer chain length. The optimal and most effective particle size for compost-derived biochar was 0.125–0.149 mm, highlighting the importance of biochar's physical and chemical properties in the adsorption process. The ideal quantity of biochar for maximizing PFDA adsorption was 43.75 mg, which required less biochar amount than PFNA, demonstrating higher performance in the competitive adsorption process involving PFNA. Deep neural network (DNN) models were applied, yielding accurate predictions of PFCA adsorption efficiencies, with the models' performance closely aligning with the experimental data. The incorporation of machine learning, enhanced by noise injection techniques, improved the accuracy of these predictions. Evaluation metrics demonstrated that the models achieved excellent coefficients of determination (R^2), with the highest recorded at 0.999, and marked by 0.9962 in the testing phase, indicating a negligible decline in predictive capability from training to testing. The comparison of RMSE and MAE between training and testing phases revealed slight increases, which illustrate the models' robustness and the effectiveness of noise injection in maintaining high predictive accuracy under varied data conditions and preventing the model from overfit.

In future research, expanding the variety of biochar types from different sources could provide a broader understanding of biochar's performance. Additionally, investigating the environmental impact associated with producing and using biochar for PFCA removal would offer valuable insights into the overall sustainability of this approach. Furthermore, exploring the integration of biochar with other technologies for both the adsorption and degradation of PFCAs could pave the way for more comprehensive removal strategies.

Limitations of the study

Despite the promising results presented in this study, several limitations must be acknowledged. Firstly, the experiments were conducted under controlled laboratory conditions, which may not fully represent the complexities of real-world water treatment systems. Variations in water chemistry, temperature, and the presence of competing contaminants in natural environments could influence biochar's adsorption efficiency. Secondly, while two types of biochar were tested, the scope of this study did not encompass a broader range of biochar types or sources that may offer differing adsorptive properties. Additionally, the machine learning models used for predictive analysis were trained on a relatively limited dataset, and their performance may vary when applied to more diverse and complex datasets. These limitations highlight areas for future research to optimize biochar-based PFCA removal in real-world applications.

RESOURCE AVAILABILITY

Lead contact

Further information and requests for resources should be directed to the lead contact, Prof. Satinder Kaur Brar (satinderbrar@lassonde.yorku.ca).

Materials availability

This study did not generate new unique reagents.

Data and code availability

- All codes used in this article will be made available upon request to the lead contact.
- The data supporting this study will be available upon request from the corresponding author.
- Any additional information required to reanalyze the data reported in this article is available from the lead contact upon reasonable request.

ACKNOWLEDGMENTS

This research was funded by the Natural Sciences and Engineering Research Council of Canada (Discovery Grant 23451, NSERC Alliance Option-2 Grants MISSED Project, ALLRP 571066–21, Alliance Option-1, ALLRP 566573 - 21). We would also like to thank James and Joanne Love Chair in Environmental Engineering and Char Technologies Inc., for their financial support.

AUTHOR CONTRIBUTIONS

S.N.: methodology, investigation, writing original draft and editing, and formal analysis. A.T.: artificial intelligence section, modeling, writing, and interpretation. R.P.: revising and reviewing, data interpretation. S.K.B.: supervision, conceptualization, methodology, review and editing, and funding acquisition. All authors interpreted the results, reviewed, edited, and approved the final version of the article.

DECLARATION OF INTERESTS

The authors declare no competing interests.

STAR★METHODS

Detailed methods are provided in the online version of this paper and include the following:

SUPPLEMENTAL INFORMATION

Supplemental information can be found online at https://doi.org/10.1016/j.isci.2024.111140.

Received: June 6, 2024
Revised: September 3, 2024
Accepted: October 7, 2024
Published: October 10, 2024

REFERENCES

1. Cordner, A., De La Rosa, V.Y., Schaider, L.A., Rudel, R.A., Richter, L., and Brown, P. (2019). Guideline levels for PFOA and PFOS in drinking water: the role of scientific uncertainty, risk assessment decisions, and social factors. J. Expo. Sci. Environ. Epidemiol. *29*, 157–171. https://doi.org/10.1038/S41370-018-0099-9.
2. Wang, Y., Niu, J., Zhang, L., and Shi, J. (2014). Toxicity assessment of perfluorinated carboxylic acids (PFCAs) towards the rotifer Brachionus calyciflorus. Sci. Total Environ. *491*, 266–270. https://doi.org/10.1016/J.SCITOTENV.2014.02.028.
3. Ross, I., Mcdonough, J., Miles, J., Storch, P., Thelakkat Kochunarayanan, P., Kalve, E., Hurst, J., S Dasgupta, S., and Burdick, J. (2018). A review of emerging technologies for remediation of PFASs. Remed. J. *28*, 101–126. https://doi.org/10.1002/rem.21553.
4. Zango, Z.U., Ethiraj, B., Al-Mubaddel, F.S., Alam, M.M., Lawal, M.A., Kadir, H.A., Khoo, K.S., Garba, Z.N., Usman, F., Zango, M.U., and Lim, J.W. (2023). An overview on human exposure, toxicity, solid-phase microextraction and adsorptive removal of perfluoroalkyl carboxylic acids (PFCAs) from water matrices. Environ. Res. *231*, 116102. https://doi.org/10.1016/J.ENVRES.2023.116102.
5. Crone, B.C., Speth, T.F., Wahman, D.G., Smith, S.J., Abulikemu, G., Kleiner, E.J., and Pressman, J.G. (2019). Occurrence of Per- and Polyfluoroalkyl Substances (PFAS) in Source Water and Their Treatment in Drinking Water. Crit. Rev. Environ. Sci. Technol. *49*, 2359–2396. https://doi.org/10.1080/10643389.2019.1614848.
6. Rahman, M.F., Peldszus, S., and Anderson, W.B. (2014). Behaviour and fate of perfluoroalkyl and polyfluoroalkyl substances

(PFASs) in drinking water treatment: A review. Water Res. *50*, 318–340. https://doi.org/10.1016/J.WATRES.2013.10.045.

7. Nzeribe, B.N., Crimi, M., Mededovic Thagard, S., and Holsen, T.M. (2019). Physico-Chemical Processes for the Treatment of Per- And Polyfluoroalkyl Substances (PFAS): A review. Crit. Rev. Environ. Sci. Technol. *49*, 866–915. https://doi.org/10.1080/10643389.2018.1542916.
8. Dabbaghi, F., Sadeghi-Nik, A., Libre, N.A., and Nasrollahpour, S. (2021). Characterizing fiber reinforced concrete incorporating zeolite and metakaolin as natural pozzolans. Structures *34*, 2617–2627. https://doi.org/10.1016/J.ISTRUC.2021.09.025.
9. Dabbaghi, F., Fallahnejad, H., Nasrollahpour, S., Dehestani, M., and Yousefpour, H. (2021). Evaluation of fracture energy, toughness, brittleness, and fracture process zone properties for lightweight concrete exposed to high temperatures. Theor. Appl. Fract. Mech. *116*, 103088. https://doi.org/10.1016/J.TAFMEC.2021.103088.
10. Kaboré, H.A., Vo Duy, S., Munoz, G., Méité, L., Desrosiers, M., Liu, J., Sory, T.K., and Sauvé, S. (2018). Worldwide drinking water occurrence and levels of newly-identified perfluoroalkyl and polyfluoroalkyl substances. Sci. Total Environ. *616*, 1089–1100. https://doi.org/10.1016/J.SCITOTENV.2017.10.210.
11. Arvaniti, O.S., and Stasinakis, A.S. (2015). Review on the occurrence, fate and removal of perfluorinated compounds during wastewater treatment. Sci. Total Environ. *524*, 81–92. https://doi.org/10.1016/J.SCITOTENV.2015.04.023.
12. Du, Z., Deng, S., Bei, Y., Huang, Q., Wang, B., Huang, J., and Yu, G. (2014). Adsorption behavior and mechanism of perfluorinated compounds on various adsorbents-A review. J. Hazard Mater. *274*, 443–454. https://doi.org/10.1016/J.JHAZMAT.2014.04.038.
13. Du, Z., Deng, S., Chen, Y., Wang, B., Huang, J., Wang, Y., and Yu, G. (2015). Removal of perfluorinated carboxylates from washing wastewater of perfluorooctanesulfonyl fluoride using activated carbons and resins. J. Hazard Mater. *286*, 136–143. https://doi.org/10.1016/J.JHAZMAT.2014.12.037.
14. Nasrollahpour, S., Kebria, D.Y., Ghavami, M., and Ghasemi-Fare, O. (2020). Application of Organically Modified Clay in Removing BTEX from Produced Water. Geo-Congress *148*, 275–283. https://doi.org/10.1061/9780784482827.031.
15. Zhang, Q., Deng, S., Yu, G., and Huang, J. (2011). Removal of perfluorooctane sulfonate from aqueous solution by crosslinked chitosan beads: Sorption kinetics and uptake mechanism. Bioresour. Technol. *102*, 2265–2271. https://doi.org/10.1016/J.BIORTECH.2010.10.040.
16. Chularueangaksorn, P. (2013). Study on Effective Adsorption Conditions for Perfluorinated Compounds (PFCs) Removal in Municipal and Industrial Wastewaters in Thailand and Japan. https://doi.org/10.14989/DOCTOR.K17932.
17. Rattanaoudom, R., Visvanathan, C., and Boontanon, S. (2012). Removal of Concentrated PFOS and PFOA in Synthetic Industrial Wastewater by Powder Activated Carbon and Hydrotalcite. J.Water.Sustain *2*, 245–258.
18. Karimaei, M., Dabbaghi, F., Dehestani, M., and Rashidi, M. (2021). Estimating Compressive Strength of Concrete Containing Untreated Coal Waste Aggregates Using Ultrasonic Pulse Velocity. Materials *14*, 647. https://doi.org/10.3390/MA14030647.
19. Schaefer, A. (2006). Perfluorinated surfactants contaminate German waters. Environ. Sci. Technol. *40*, 7108–7109. https://doi.org/10.1021/es062811u.
20. Xiao, X., Ulrich, B.A., Chen, B., and Higgins, C.P. (2017). Sorption of Poly- and Perfluoroalkyl Substances (PFASs) Relevant to Aqueous Film-Forming Foam (AFFF)-Impacted Groundwater by Biochars and Activated Carbon. Environ. Sci. Technol. *51*, 6342–6351. https://doi.org/10.1021/ACS.EST.7B00970/ASSET/IMAGES/LARGE/ES-2017-00970R_0005.JPEG.
21. Gęca, M., Wiśniewska, M., and Nowicki, P. (2022). Biochars and activated carbons as adsorbents of inorganic and organic compounds from multicomponent systems - A review. Adv. Colloid Interface Sci. *305*, 102687. https://doi.org/10.1016/J.CIS.2022.102687.
22. Yaashikaa, P.R., Kumar, P.S., Varjani, S., and Saravanan, A. (2020). A critical review on the biochar production techniques, characterization, stability and applications for circular bioeconomy. Biotechnology Reports *28*, e00570. https://doi.org/10.1016/J.BTRE.2020.E00570.
23. Liu, N., Wu, C., Lyu, G., and Li, M. (2021). Efficient adsorptive removal of short-chain perfluoroalkyl acids using reed straw-derived biochar (RESCA). Sci. Total Environ. *798*, 149191. https://doi.org/10.1016/J.SCITOTENV.2021.149191.
24. Dabbaghi, F., Nasrollahpour, S., Dehestani, M., and Yousefpour, H. (2022). Optimization of Concrete Mixtures Containing Lightweight Expanded Clay Aggregates Based on Mechanical, Economical, Fire-Resistance, and Environmental Considerations. J. Mater. Civ. Eng. *34*, 04021445. https://doi.org/10.1061/(ASCE)MT.1943-5533.0004083.
25. Kim, J., Kim, D.G., and Ryu, K.H. (2023). Enhancing Response Surface Methodology through Coefficient Clipping Based on Prior Knowledge. Processes *11*, 3392. https://doi.org/10.3390/PR11123392.
26. Dabbaghi, F., Tanhadoust, A., Nehdi, M.L., Dehestani, M., and Yousefpour, H. (2022). Investigation on optimal lightweight expanded clay aggregate concrete at high temperature based on deep neural network. Struct. Concr. *23*, 3727–3753. https://doi.org/10.1002/SUCO.202100694.
27. Tanhadoust, A., Emadi, S.A.A., Nasrollahpour, S., Dabbaghi, F., and Nehdi, M.L. (2023). Optimal design of sustainable recycled rubber-filled concrete using life cycle assessment and multi-objective optimization. Construct. Build. Mater. *402*, 132878. https://doi.org/10.1016/J.CONBUILDMAT.2023.132878.
28. Dabbaghi, F., Tanhadoust, A., Nehdi, M.L., Nasrollahpour, S., Dehestani, M., and Yousefpour, H. (2021). Life cycle assessment multi-objective optimization and deep belief network model for sustainable lightweight aggregate concrete. J. Clean. Prod. *318*, 128554. https://doi.org/10.1016/J.JCLEPRO.2021.128554.
29. Amiri, H., Azadi, S., Karimaei, M., Sadeghi, H., and Dabbaghi, F. (2022). Multi-objective optimization of coal waste recycling in concrete using response surface methodology. J. Build. Eng. *45*, 103472. https://doi.org/10.1016/J.JOBE.2021.103472.
30. Mohammad, S., Fitzgerald, J., Robinson, R.L., and Gasem, K.A.M. (2009). Experimental Uncertainties in Volumetric Methods for Measuring Equilibrium Adsorption. Energy Fuels *23*, 2810–2820. https://doi.org/10.1021/ef8011257.
31. Sepideh, N., Yousefi, K.D., L, N.M., Amin, T., and Mohammad, G. (2023). Remediation of NAPL-Contaminated Brackish Water by Synthesized Organoclay: Experimental Analysis and BNN Predictive Model. J Hazard Toxic Radioact Waste *27*, 04023028. https://doi.org/10.1061/JHTRBP.HZENG-1212.
32. Onyelowe, K.C., Kontoni, D.P.N., Oyewole, S., Apugo-Nwosu, T., Nasrollahpour, S., Soleymani, A., Pilla, S.R.M., Jahangir, H., and Dabbaghi, F. (2023). Compressive strength optimization and life cycle assessment of geopolymer concrete using machine learning techniques. E3S Web Conf. *436*, 08009. https://doi.org/10.1051/E3SCONF/202343608009.
33. Labach, A., Salehinejad, H., and Valaee, S. (2019). Survey of dropout methods for deep neural networks. Preprint at arXiv. https://doi.org/10.48550/arXiv.1904.13310.
34. Banik, C., Lawrinenko, M., Bakshi, S., and Laird, D.A. (2018). Impact of Pyrolysis Temperature and Feedstock on Surface Charge and Functional Group Chemistry of Biochars. J. Environ. Qual. *47*, 452–461. https://doi.org/10.2134/JEQ2017.11.0432.
35. Leung, S.C.E., Wanninayake, D., Chen, D., Nguyen, N.T., and Li, Q. (2023). Physicochemical properties and interactions of perfluoroalkyl substances (PFAS) - Challenges and opportunities in sensing and remediation. Sci. Total Environ. *905*, 166764. https://doi.org/10.1016/J.SCITOTENV.2023.166764.
36. Zheng, Q.F., Wang, Y.H., Sun, Y.G., Niu, H.H., Zhou, J.R., Wang, Z.M., and Zhao, J. (2014). Study on Structural Properties of Biochar under Different Materials and Carbonized by FTIR. Guang Pu Xue Yu Guang Pu Fen Xi/Spectroscopy and Spectral Analysis *34*, 962–966. https://doi.org/10.3964/J.ISSN.1000-0593(2014)04-0962-05.
37. Liu, Y., He, Z., and Uchimiya, M. (2015). Comparison of Biochar Formation from Various Agricultural By-Products Using FTIR Spectroscopy. Mod. Appl. Sci. *9*, 246. https://doi.org/10.5539/mas.v9n4p246.
38. Aboughaly, M., and Fattah, I.M.R. (2023). Production of Biochar from Biomass Pyrolysis for Removal of PFAS from Wastewater and Biosolids: A Critical Review. https://doi.org/10.20944/PREPRINTS202304.0309.V1.
39. Krahn, K.M., Cornelissen, G., Castro, G., Arp, H.P.H., Asimakopoulos, A.G., Wolf, R., Holmstad, R., Zimmerman, A.R., and Sørmo, E. (2023). Sewage sludge biochars as effective PFAS-sorbents. J. Hazard Mater. *445*, 130449. https://doi.org/10.1016/J.JHAZMAT.2022.130449.
40. Behnami, A., Pourakbar, M., Ayyar, A.S.R., Lee, J.W., Gagnon, G., and Zoroufchi

Benis, K. (2024). Treatment of aqueous per- and poly-fluoroalkyl substances: A review of biochar adsorbent preparation methods. Chemosphere *357*, 142088. https://doi.org/10.1016/J.CHEMOSPHERE.2024.142088.

41. Guo, W., Huo, S., Feng, J., and Lu, X. (2017). Adsorption of perfluorooctane sulfonate (PFOS) on corn straw-derived biochar prepared at different pyrolytic temperatures. J. Taiwan Inst. Chem. Eng. *78*, 265–271. https://doi.org/10.1016/J.JTICE.2017.06.013.
42. Zhang, Y., Tan, X., Lu, R., Tang, Y., Qie, H., Huang, Z., Zhao, J., Cui, J., Yang, W., and Lin, A. (2022). Enhanced Removal of Polyfluoroalkyl Substances by Simple Modified Biochar: Adsorption Performance and Theoretical Calculation. ACS ES and T Water *3*, 816–826. https://doi.org/10.1021/ACSESTWATER.2C00597/ASSET/IMAGES/LARGE/EW2C00597_0008.JPEG.
43. Ahmed, M.B., Johir, M.A.H., McLaughlan, R., Nguyen, L.N., Xu, B., and Nghiem, L.D. (2020). Per- and polyfluoroalkyl substances in soil and sediments: Occurrence, fate, remediation and future outlook. Sci. Total Environ. *748*, 141251. https://doi.org/10.1016/J.SCITOTENV.2020.141251.
44. Vo, H.N.P., Nguyen, T.M.H., Ngo, H.H., Guo, W., Shukla, P., Guo, W., and Shukla, P. (2022). Biochar sorption of perfluoroalkyl substances (PFASs) in aqueous film-forming foams-impacted groundwater. Chemosphere *286*, 131622. https://doi.org/10.1016/j.chemosphere.2021.131622.
45. Fabregat-Palau, J., Vidal, M., and Rigol, A. (2022). Examining sorption of perfluoroalkyl substances (PFAS) in biochars and other carbon-rich materials. Chemosphere *302*, 134733. https://doi.org/10.1016/J.CHEMOSPHERE.2022.134733.
46. Abdelfatah, E.R., Kang, K., Pournik, M., Shiau, B., Harwell, J., Haroun, M.R., and Rahman, M.M. (2017). Study of Nanoparticle Adsorption and Release in Porous Media Based on the DLVO Theory. In SPE Latin American and Caribbean Petroleum Engineering Conference Proceedings. https://doi.org/10.2118/185484-MS.

STAR★METHODS

KEY RESOURCES TABLE

REAGENT or RESOURCE	SOURCE	IDENTIFIER
Chemicals, peptides, and recombinant proteins		
Perfluorononanoic acid (C9HF17O2)	Thermo Fisher Scientific	CAS: 375-95-1
Perfluorodecanoic acid (C10HF19O2)	Thermo Fisher Scientific	CAS: 335-76-2
Methanol	Fisher Scientific	CAS: 67-56-1
Biochar from composted food waste	CHAR Technologies Inc., Toronto, Canada	composted food waste and
Biochar from pine wood shavings	CHAR Technologies Inc., Toronto, Canada	pine wood shavings
Software and algorithms		
Excel	Microsoft 365	https://www.microsoft.com/es-ec/
Origin 2023	OriginLab	https://www.originlab.com
MATLAB R2024a	MathWorks	https://www.mathworks.com
Other		
FTIR Spectrometer	Bruker Alpha-P, USA	https://tinyurl.com/55ak8zas
Elemental Analyzer	Thermo Flash Smart V	https://tinyurl.com/yzzwrnrm
UPLC system (Waters) coupled with a ZenoToF 7600 (Sciex) mass spectrometer.	ACQUITY M-class	https://tinyurl.com/322wpcff

EXPERIMENTAL MODEL AND STUDY PARTICIPANT DETAILS

Experimental setup

Biochar preparation

Two types of biochar were used in this study: wood-derived and compost-derived. Both biochars were sourced from CHAR Technologies Inc. Toronto, Canada and prepared under controlled pyrolysis conditions. The specific temperatures and durations of pyrolysis were 600°C for 40 min and 800°C for 30 min, respectively. Post-pyrolysis, the biochars were ground and sieved to obtain particles of uniform size.

PFCA solutions

Preparation

Stock solutions of PFNA and PFDA were prepared in deionized water at concentrations of 1000 μg/L. Working solutions were then diluted to the desired concentrations for experimental use.

METHOD DETAILS

Adsorption experiments

Biochar characterization

Biochar was ground and sifted into four size ranges (0.063–1 mm) for analysis. FTIR spectroscopy was employed to analyze surface chemical composition, focusing on C, N, O, and H functional groups. Quantification of C, N, H, and S was performed using a Thermo Flash Smart V Elemental Analyzer.

Screening and selection of Biochar

An initial screening experiment was conducted using 25 mg of each biochar in 25 mL of Milli-Q water, spiked with PFNA and PFDA at various concentrations (10–500 μg/L). The mixtures were incubated for 24 h and centrifuged, and PFCA concentrations were determined using LC/MS.

Adsorptive kinetics of PFCAs

Adsorption kinetics were assessed using 25 mg of biochar in 50 mL of Milli-Q water, spiked with 100 μg/L of PFCAs. Samples were taken at various intervals over 72 h, centrifuged, and analyzed by LC/MS to observe adsorption trends.

Batch sorption tests

Adsorption experiments were designed using Response Surface Methodology (RSM) and Central Composite Design (CCD). Various parameters were explored, including biochar particle size, PFCA concentrations, and biochar quantities. Samples were incubated and analyzed at different time intervals using LC/MS.

Sample extraction and analysis

PFCA concentrations were quantified using an ACQUITY M-class UPLC system coupled with a ZenoToF 7600 mass spectrometer. The LC-MS/MS system operated with a C18 column and a gradient mobile phase, with ion optics set for negative ion electrospray mode. Quantitative measurements were recorded using high-resolution multiple reaction monitoring (MRM-HR).

Data analysis

Excel 2016

The data obtained from the adsorption experiments were processed using Microsoft Excel 2016 for initial analysis and graph plotting. Data such as adsorption capacity and percentage removal were calculated.

Origin 2022

Graphical representations, including adsorption isotherms and kinetics, were plotted using Origin 2022 to ensure precise and professional visualization of the results.

MATLAB R2024a

Advanced data analysis, including the implementation of deep neural networks (DNNs) for predictive modeling, was performed using MATLAB R2024a. Noise injection was incorporated into the model to account for uncertainties and to prevent overfitting. The neural network architecture was optimized using a grid search method, focusing on the number of layers, nodes, learning rate, and activation functions.

Quality control

Reproducibility

All experiments were conducted in triplicate to ensure reproducibility. The standard deviation and standard error were calculated to assess the consistency of the results.

QUANTIFICATION AND STATISTICAL ANALYSIS

Model validation

The predictive model's performance was evaluated using mean squared error (MSE) and coefficient of determination (R^2) metrics. A 10-fold cross-validation was performed to ensure the robustness of the model.